Control of PEM Fuel Cell Distributed Generation Systems

C. Wang, *Student Member, IEEE*, M. H. Nehrir, *Senior Member, IEEE*, and H. Gao, *Member, IEEE*

***Abstract*—This paper presents modeling, controller design, and simulation study of a proton exchange membrane fuel cell (PEMFC) distributed generation (DG) system. The overall configuration of the PEMFC DG system is given, dynamic models for the PEMFC power plant and its power electronic interfacing are briefly described, and controller design methodologies for the power conditioning units to control the power flow from the fuel cell power plant to the utility grid are presented.**

A MATLAB/Simulink simulation model is developed for the PEMFC DG system by combining the individual component models and the controllers designed for the power conditioning units. Simulation results are given to show the overall system performance including load-following and fault-handling capability of the system.

***Index Terms*—Control, distributed generation (DG), interfacing, modeling, PEM fuel cell (PEMFC).**

I. Introduction

THE EVER-INCREASING energy consumption and the rising public awareness for environmental protection have created increased interest in green (i.e., renewable and fuel-cell-based) power generation systems. Moreover, due to steady progress in power deregulation and utility restructuring and because tight constraints are imposed on the construction of new transmission lines for long-distance power transmission, interest in distributed generation (DG) systems installed near load centers is increasing.

Fuel cells are static energy conversion devices that convert the chemical energy of fuel directly into electrical energy. They show great promise to be an important DG source of the future due to their many advantages, such as high efficiency, zero or low emission (of pollutant gases), and flexible modular structure. Fuel cell DG systems can be strategically placed at any site in a power system (normally at the distribution level) for grid reinforcement, thereby deferring or eliminating the need for system upgrades and improving system integrity, reliability, and efficiency. When connected to a utility grid, important operation and performance requirements are imposed on fuel cell DG systems. For example, they should be able to deliver a preset amount of real and reactive power to the grid or be able to follow a time-varying load profile [2], [6], [27]. Therefore, proper controllers need to be designed for a fuel cell DG system to make its performance characteristics as desired.

Among several types of fuel cells, proton exchange membrane fuel cells (PEMFC), solid oxide fuel cells (SOFC), and molten carbonate fuel cells (MCFC) are likely to be used in DG applications. To study the performance characteristics of fuel cell DG systems, accurate models of fuel cells are needed [1]–[8]. Moreover, models for the interfacing power electronic circuits in a fuel cell DG system are also needed to design controllers for the overall system to improve its performance and to meet certain operation requirements [7]–[9].

This paper presents the modeling and control of a PEMFC DG system with real and reactive power control capability. The fuel cell power plant is interfaced with the utility grid via boost dc/dc converters and a three-phase pulsewidth modulation (PWM) inverter. A validated PEMFC dynamic model, reported in [1], is used in this paper. The models for the boost dc/dc converter and the three-phase inverter together with an *LC* filter and transmission lines are also addressed. The controller design methodologies for the dc/dc converters and the three-phase inverter are also presented for the proposed fuel cell DG system. Based on the individual component models developed and the controllers designed, a simulation model of the PEMFC DG system has been built in MATLAB/Simulink using SimPowerSystems block-set. Simulation results show that the real and reactive power from the fuel cell DG system to the utility grid can be controlled as desired. The results also show that the fuel cell DG system is capable of load-following and remaining stable under severe electrical faults.

II. System Description

To meet the system operational requirements, a fuel cell DG system needs to be interfaced through a set of power electronic devices. The interface is very important as it affects the operation of the fuel cell system as well as the power grid.

Various power electronic circuits have been proposed in recent work to interface different energy sources with the utility grid [9]–[16]. Pulse-width modulated voltage source inverters (VSI) are widely used to interconnect a fuel cell energy system to a utility grid for real and reactive power control purposes [9], [11], [15], [16]. In addition, fuel cell systems normally need boost dc/dc converters to adapt the fuel cell output voltage to the desired inverter input voltage and smooth the fuel cell output current [17], [18].

Fig. 1 shows the schematic diagram of the fuel cell DG system proposed in this paper. The system configuration ratings and parameters are given in Table I. The PEMFC power plant consists of ten fuel cell arrays connected in parallel. Each array

Manuscript received November 3, 2004; revised May 5, 2005, This work was supported in part by the National Science Foundation under Grant ECS-0135229 and the Department of Energy under Contract 3917 (413060-A) administered by the Pacific Northwest National under Laboratory through the HiTEC Center at Montana State University. Paper no. TEC-00312-2004.

The authors are with the Department of Electrical and Computer Engineering, Montana State University, Bozeman, MT 59717 USA (e-mail: cwang@montana.edu; hnehrir@ece.montana.edu).

Digital Object Identifier 10.1109/TEC.2005.860404

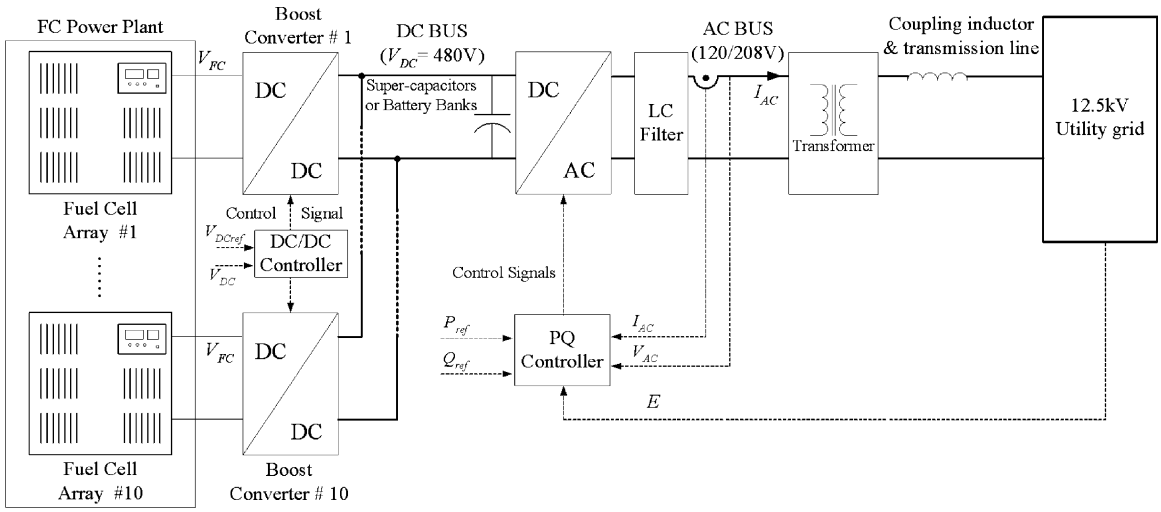

Fig. 1. Block diagram of a fuel cell distributed generation system.

TABLE I
CONFIGURATION PARAMETERS OF THE PROPOSED SYSTEM

PEMFC Power Plant	216V/480kW Ten 48-kW FC arrays are connected in parallel
PEMFC Array	216 V/48 kW, consisting of 8(series) × 12 (parallel) 500-W fuel cell stacks
Boost dc/dc Converter	200 V/480 V, 50 kW each. 10 units connected in parallel.
3-phase dc/ac Inverter	480 V dc/208 V ac, 500 kW
LC Filter	L_f = 0.15 mH, C_f = 306.5 uF
Step-Up Transformer	V_n = 208 V/12.5 kV, S_n = 500 kW $R_1 = R_2$ = 0.005 p.u., $X_1 = X_2$ = 0.025 p.u.
Coupling Inductor	X_c = 50 Ω
Transmission Line	0.5 km ACSR 6/0 R = 2.149 Ω/km, X = 0.5085 Ω/km
DC Bus Voltage	480 V
AC Bus Voltage	120 V/208 V

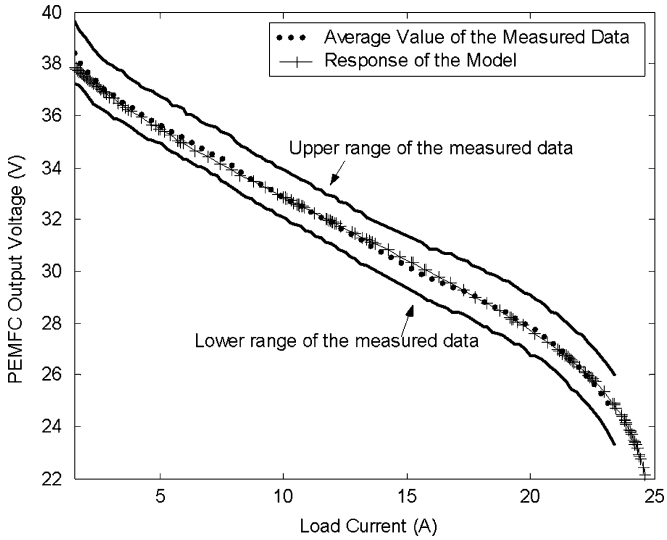

Fig. 2. PEMFC V–I characteristic: Comparison of model response with experimental data [1].

is rated at 48 kW, for a total of 480 kW. A boost converter is used to adapt the output voltage of each fuel cell array to the dc bus voltage. In this paper, the dc bus voltage (dc/dc converter output) is chosen as $V_{\rm DC} = 480$ V, which is mainly determined by the inverter ac output voltage and the voltage drop across the LC filter. The following equation should be satisfied between the dc side and ac side voltages of the inverter [15]:

$$\frac{\sqrt{3}}{2\sqrt{2}} m_a V_{\rm DC} \geq \sqrt{(V_{\rm AC,LL})^2 + 3(\omega L_f I_{\max})^2} \qquad (1)$$

where $V_{\rm DC}$ is the dc bus voltage, $V_{\rm AC,LL}$ is the ac side line-line rms voltage, L_f is the filter inductance, $I_{\max}$ is the root mean square (rms) value of maximum ac load current $(I_{\rm AC})$, and m_a is the modulation index of the inverter. Linear PWM is used for the inverter, i.e., $m_a \leq 1.0$, in this paper.

For a boost converter, the higher the duty ratio (or the larger the voltage difference between the input and the output), the lower is the efficiency [16]. In this paper a duty ratio around 55% is used for the dc/dc converter at the fuel cell's rated operating point. The approximate desired input voltage for the dc/dc converter can be obtained to be $[(1 - 0.55) \times V_{\rm DC} = 216$ V]. According to the output voltage versus load current (V–I) characteristics of the PEMFC, given in Fig. 2, when its load current is over 23 A the fuel cell is in concentration zone, which should be avoided [19], [20]. To leave some safe margin, the fuel cell is operated around the point where its current is 20 A (rated operating point) and its output voltage $(V_{\rm FC,cell})$ is about 27 V. Therefore, the number of fuel cell stacks we need to connect in a series to get a voltage of 216 V is

$$N_s = \frac{V_{\rm FC}}{V_{\rm FC,cell}} = \frac{216}{27} = 8. \qquad (2)$$

The number of fuel cell series stacks needed to compose a 48-kW fuel cell array is

$$N_p = \frac{P_{\rm array}}{N_s \times P_{\rm stack}} = \frac{48\ {\rm kW}}{8 \times 0.5\ {\rm kW}} = 12. \qquad (3)$$

Therefore, each fuel cell array is composed of 8×12 stacks with the power rating of 48 kW.

Supercapacitors or battery banks are connected to the dc bus to provide storage capability and fast dynamic response to load transients. A three-phase six-switch inverter interfaces the dc bus with a 120 V/208 V ac power system. An *LC* filter is connected to the output of the inverter to reduce the harmonics introduced by the inverter. A 208-V/12.5-kV step-up transformer connects the fuel cell power system to the utility grid through a coupling inductor and a short transmission line. The coupling inductor is needed to control the real and reactive power flow between the fuel cell DG system and the utility grid and to limit disturbance and fault currents.

The controllers for the boost dc/dc converters are designed to keep the dc bus voltage within an acceptable band ($\pm 5\%$ in this paper). Therefore, the input to the three-phase inverter can be considered a fairly good constant voltage source. The inverter controller controls the real and reactive power flows to the utility grid. P, Q power flows follow their respective reference values, which can be set either as fixed values or to follow a certain load demand.

III. Dynamic Models for PEMFC and Power Electronic Devices

This section describes the dynamic models for the main components of the system shown in Fig. 1, namely for the PEMFC power plant, the dc/dc converters and the three-phase inverter.

A. Dynamic Model for the PEMFC Power Plant

PEMFCs, one of the most developed fuel cells, show great promise both in transportation and in stationary power generation applications. To investigate the dynamic characteristics of a PEMFC power plant under load transients, it is necessary to use a dynamic PEMFC model. The model of PEMFC power plant used in this study is based on the dynamic PEMFC stack model developed and validated in [1]. This physically based model uses equivalent electrical circuits to represent the electrochemical and thermodynamic phenomena inside the PEMFC. The model was validated by experimental data measured from an Avista Labs SR-12 500-W PEMFC stack. It is an autonomous model operated under constant channel pressure with no control on the input fuel flow into the fuel cell. The fuel cell will adjust the input fuel flow according to its load current to keep the channel pressure constant.

Fig. 2 shows the (V–I) characteristic curve of the 500-W PEMFC model compared with the experimental data [1]. This characteristic curve can be divided into three regions. The voltage drop across the fuel cell associated with low currents is due to the activation loss inside the fuel cell, the voltage drop in the middle of the curve (which is approximately linear) is due to the ohmic loss in the fuel cell stack, and as a result of the concentration loss, the output voltage at the end of the curve will drop sharply as the load current increases [19], [20].

The dynamic property of PEMFC depends mainly on the following three aspects: double-layer charging effects, fuel and oxidant flow delays, and thermodynamic characteristics inside the fuel cell. The dynamic response of PEMFC is dominated by the double-layer charging effects in the short-time range (less than 1 s) and by the fuel and oxidant flow delays and thermodynamic characteristics inside the fuel cell in the long-time range (several minutes) [1], [20]. The dynamic response of the model (fuel cell output voltage vs. time) to step load changes in the short-time range is shown in Fig. 3. It is noted from this figure that the response of the model agrees well with the measured data. For further details about the model development, the reader is referred to [1].

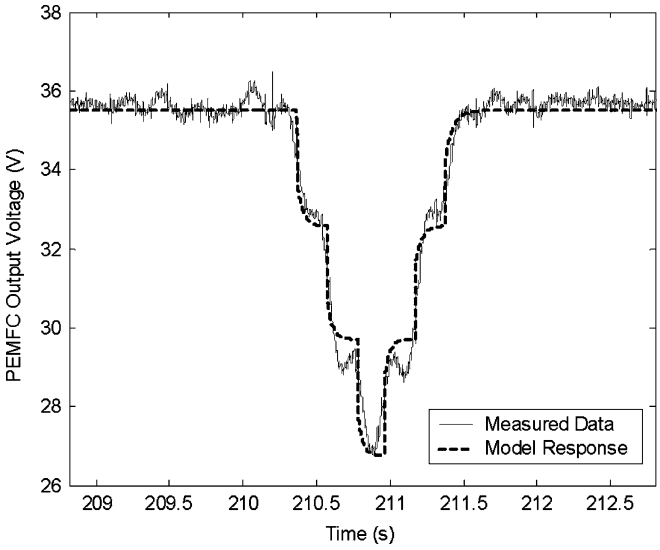

Fig. 3. PEMFC dynamic response in short time range: Comparison of model response with experimental data [1].

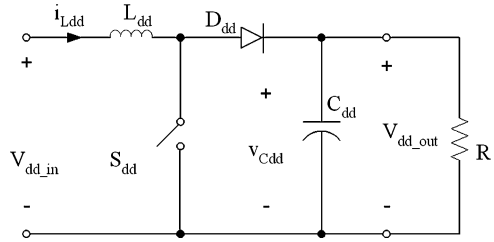

Fig. 4. Boost dc/dc converter.

B. State Space Model of Boost dc/dc Converter

A boost dc/dc converter, shown in Fig. 4 [15], can be used to convert the fuel cell output voltage to the desired dc bus voltage. A state space averaging technique, proposed by Middlebrook and Cúk [15], is widely used to develop linear state space models for converters. The small signal state space model for the boost dc/dc converter can then be obtained as follows:

$$\begin{aligned} \dot{\tilde{x}} &= A_d \tilde{x} + B_d \tilde{d} \\ \tilde{v}_{dd\_\mathrm{out}} &= C^T \tilde{x} \end{aligned} \tag{4}$$

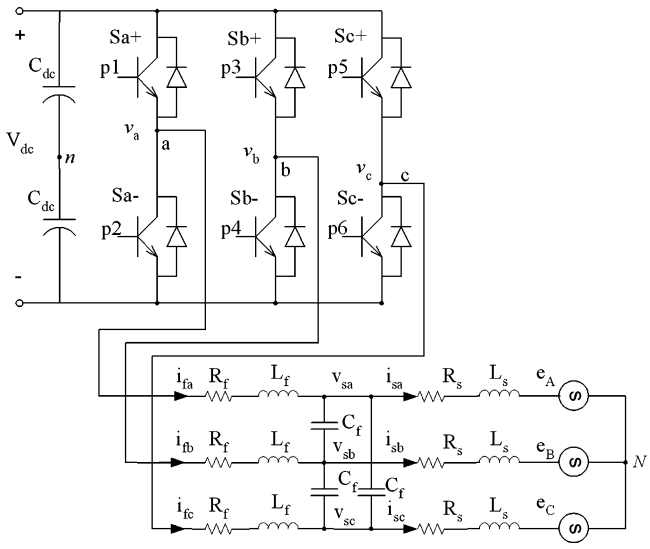

Fig. 5. Three-phase dc/ac voltage source inverter.

where

$$\tilde{x} = \begin{bmatrix} \tilde{i}_{\mathrm{Ldd}} \\ \tilde{v}_{\mathrm{cdd}} \end{bmatrix}, \quad A_d = \begin{bmatrix} 0 & \frac{-(1-D)}{L_{\mathrm{dd}}} \\ \frac{1-D}{C_{\mathrm{dd}}} & \frac{-1}{RC_{\mathrm{dd}}} \end{bmatrix}, \quad B_d = \begin{bmatrix} \frac{X_2}{L_{\mathrm{dd}}} \\ \frac{-X_1}{C_{\mathrm{dd}}} \end{bmatrix}.$$

Where $C^T = [0,1]$, X_1, and X_2 are the steady-state values of x_1 and x_2 respectively, and D is the pulse duty ratio at the rated operating point. The symbol " $\sim$ " is used to denote small perturbation signals.

C. State Space Model of Three-Phase Inverter

A three-phase six-switch PWM VSI is used to convert the power available at the dc bus to ac power. Fig. 5 shows the main circuit of the three-phase voltage source inverter connected to the utility grid through the *LC* filter (L_f and C_f) and the coupling inductor (L_s). R_f and R_s in the figure are the parasitic resistances of the filter inductor and the coupling inductor, respectively.

Using the classic electrical circuit theory and state-space averaging technique, a detailed state-space description of the inverter can be obtained [23], [24]. However, the detailed model of the inverter is too complicated to be applied directly in controller design. A simplified version of the inverter model, which is used in this paper to design controllers, is given in the Appendix.

IV. Controller Designs for Power Electronic Devices

It was shown in Figs. 2 and 3 that the output voltage of a fuel cell is a function of the load. The boost dc/dc converter adapts the fuel cell output voltage to the dc bus voltage, and the voltage controller helps regulate the output voltage within a $\pm 5\%$ tolerance band under normal operation. In this section, conventional PI controller is used for the boost dc/dc converters. In practice, a load sharing controller (not discussed in this paper) can be applied on the converters, connected in parallel, to achieve a uniform load distribution among them [28]. Also, a dq transformed two-loop current control scheme is presented for the inverter to control the real and reactive power delivered from the fuel cell power system to the grid.

TABLE II
Parameters of the Boost dc/dc Converter

L_{dd}	1.2 mH
C_{dd}	2500 μF
D_N	0.5833
R (Equivalent load)	4.608 Ω
X_1	250 A
X_2	480 V
k_{di}	20
k_{dp}	0.02

A. Controller Design for the Boost dc/dc Converter

The main components of the dc/dc converter can be determined by the prescribed technical specifications, such as the rated and peak voltage and current, input current ripple, and output voltage ripple, etc., using the classic boost dc/dc converter design procedure [15], [16]. The component values for the 48-kW dc/dc converter used in this paper are listed in Table II.

Based on the converter model in (5), a PI current controller $(k_{\mathrm{dp}} + k_{\mathrm{di}}/s)$ can be designed using the classic Bode-plot and root-locus method [21]. The parameters of the PI voltage controller are also listed in Table II.

B. Controller Design for the Three-Phase VSI

To meet the requirements for interconnecting a fuel cell system to a utility grid and control the real and reactive power flow between them, it is necessary to shape and control the inverter output voltage in amplitude, angle, and frequency [22]. In this section, a PWM controller is designed for the inverter to satisfy voltage regulation as well as to achieve real and reactive power control.

The dq transformation transfers a stationary (abc) system to a rotating $(dq0)$ system. The transformation decreases the number of control variables from 3 to 2 (component 0 will be zero) if the system is balanced. Moreover, the dq signals can be used to achieve zero tracking error control [24]. Due to these merits, dq transformation has been widely used in PWM converter/inverter control and is also applied for the inverter control in this paper.

For a fuel cell DG system, there is no flexibility for the modulation frequency of the sinusoidal PWM (SPWM) generator for the inverter—it must follow the frequency of the grid to which it is connected. The magnitude of the inverter output voltage can have a tolerance of $\pm 5\%$ with a nominal value of 1.0 p.u. [22], [25]. Therefore, the angle of the output voltage will be controlled, together with a $\pm 5\%$ magnitude adjustment, to achieve real and reactive power control.

Consider a voltage source $V_s \angle \delta$ connected to a utility grid $E \angle 0^\circ$ through a coupling impedance $R + jX$, as shown in Fig. 6. The real and reactive powers delivered to the utility

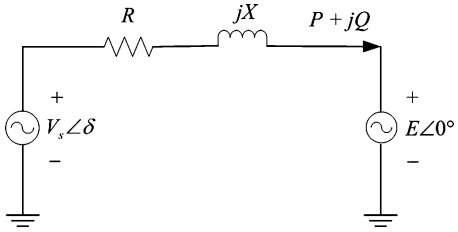

Fig. 6. Power flow between a voltage source and utility grid.

grid are [25]

$$P = \frac{EV_s}{Z}\cos(\theta_z - \delta) - \frac{E^2}{Z}\cos(\theta_z) \tag{5}$$

$$Q = \frac{EV_s}{Z}\sin(\theta_z - \delta) - \frac{E^2}{Z}\sin(\theta_z) \tag{6}$$

where $Z = \sqrt{R^2 + X^2}$ and $\theta_z = \tan^{-1}(X/R)$.

From (5) and (6), it is clear that the real and reactive powers delivered to the utility grid are completely determined by the amplitude and angle of the sending voltage source, i.e., the output voltage of the inverter. However, if the desired values of real and reactive power are given, the values of V_s and δ can be determined from (5) and (6):

$$V_s = \left[\frac{Z^2}{E^2}(P^2 + Q^2) + E^2 + 2PZ\cos(\theta_z) + 2QZ\sin(\theta_z)\right]^{\frac{1}{2}} \tag{7}$$

$$\delta = \theta_z - \cos^{-1}\left(\frac{ZP}{EV_s} + \frac{E}{V_s}\cos(\theta_z)\right). \tag{8}$$

The corresponding $dq0$ component values of V_s in (7) can be obtained through abc/dq transformation as follows:

$$\begin{bmatrix} V_d \\ V_q \\ V_0 \end{bmatrix} = T_{abc/dq}\begin{bmatrix} V_a \\ V_b \\ V_c \end{bmatrix} = T_{abc/dq}\begin{bmatrix} V_s\angle\delta \\ V_s\angle(\delta - 120°) \\ V_s\angle(\delta + 120°) \end{bmatrix} \tag{9}$$

where $T_{abc/dq}$ is the abc/dq transformation matrix. The methodology for developing the abc/dq transformation is explained in [29].

A control scheme consisting of an outer voltage regulator with an inner current control loop, reported in [23], [24], was adopted for the three-phase voltage source inverter control. The overall control system block diagram for the inverter is given in Fig. 7. The inner current control loop is designed to respond faster than the outer voltage control loop so that the two control loops can be designed independently. As a result, when dealing with the inner loop, we take the outer loop as a constant input (i.e., $I_{d,q(\mathrm{ref})}$ is constant in Fig. 7). The inner current control loop (containing the current controller block in Fig. 7) can be approximated as a simple lag block when we proceed with the outer loop. The current and voltage controllers are chosen as PI compensators. Classic Bode-plot and root-locus PI controller design procedures [21] are used to obtain the parameters for the current and voltage controllers. These parameters are listed in the Appendix as well.

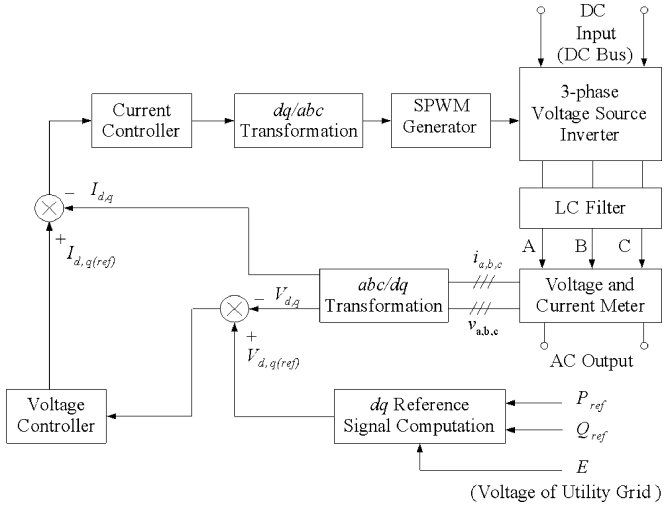

Fig. 7. Block diagram of the overall control system of the inverter.

In Fig. 7, the dq reference signal computation block, which is based on equations (7) and (8), calculates the magnitude and angle of the filtered output voltages of the inverter and then converts them into dq voltage reference signals according to (10). The abc/dq transformation block takes the current and voltage values (in abc coordinate) from the voltage and current meters and converts them into dq values. The outer voltage controller takes the error signals between the actual output voltage in dq frame $(V_{d,q})$ and the reference voltage $(V_{d,q(\mathrm{ref})})$ and generates the current reference signals $(I_{d,q(\mathrm{ref})})$ for the current control loop. The inner current controller produces the dq control signals, which are converted back into the control signals in abc coordinates through the dq/abc transformation block. These control signals are used to modulate the SPWM pulse generator to produce the proper pulses for the inverter switches (Fig. 5), which control the inverter output voltage.

The controllers given in this section for power electronic converters are designed on the basis of small-signal linearized models. Conceptually, there is no guarantee that the designed controllers will work well over a large operating range because of the nonlinearity of power electronic devices. Nevertheless, the majority of controllers for power electronic devices are linear time-invariant (LTI) that are designed on the basis of linearized models. The effectiveness of LTI controllers can be checked through simulations on more detailed (nonlinear) models than the linearized ones used for the initial controller design [30]. We have verified the validity of the proposed control schemes over a large operating range through simulations on nonlinear converter/inverter models. The simulation results will be discussed in the following section.

V. Simulation Results

The following components were used to develop a simulation model for the proposed PEMFC DG system: the dynamic model developed for PEMFC reported in [1], nonlinear models for power electronic devices from the SimPowerSystems block-set in MATLAB/Simulink, and the controllers designed

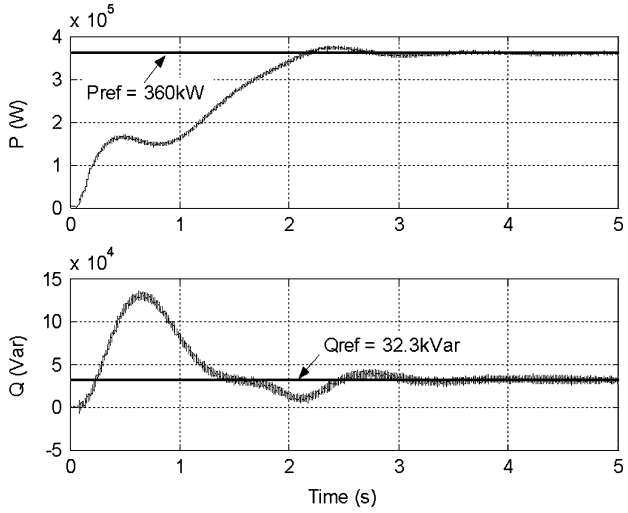

Fig. 8. P and Q delivered to the grid: Heavy loading.

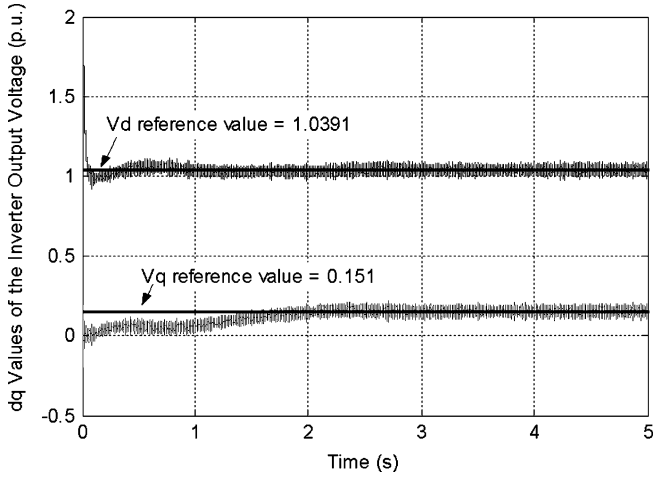

Fig. 9. dq values of the inverter output voltage under heavy load.

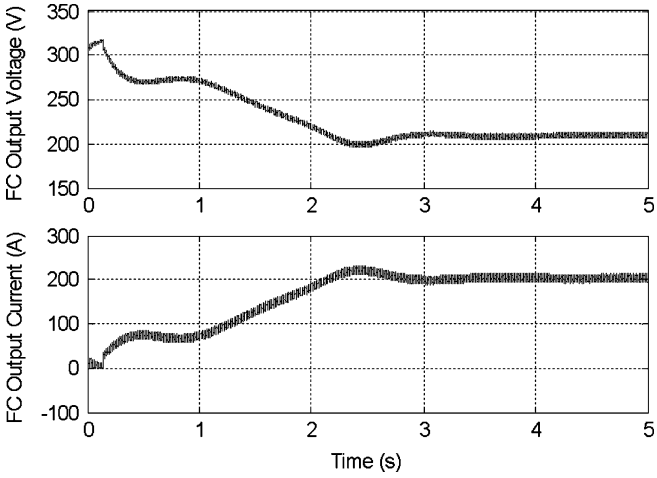

Fig. 10. Output voltage and current of each fuel cell array under heavy load.

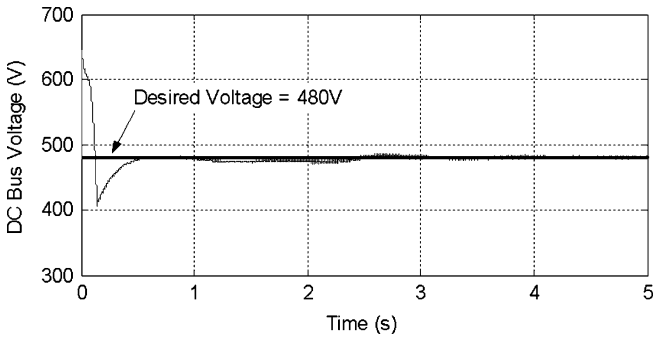

Fig. 11. DC bus voltage waveform under heavy load.

in Section IV. The system was tested under several different operating conditions to investigate its power management and load-following capabilities as well as its stability during electrical faults. Sample simulation results from the scenarios studied are given below.

A. Desired P and Q Delivered to the Grid: Heavy Loading

Normally, when a utility is under heavy load, it needs the connected DG systems (the PEMFC DG system in this case) to deliver more real power to the grid. The DG systems may also be required to deliver reactive power to the grid to help boost the grid voltage. Simulation results for such a scenario are given in this subsection.

The reference values of P and Q are set as 360 kW and 32.3 kVar with a ramp startup in 2 s for this case study. The voltage of the utility grid was set to $E = 0.98\angle 0^\circ$ p.u. Using (7) and (8), the desired magnitude and angle of the filtered output voltage of the inverter turn out to be $V_s = 1.05$p.u., $\delta = 8.2678^\circ$. Converting the values from the abc reference frame into dq coordinates yields $V_{d(\mathrm{ref})} = 1.0391$ p.u. and $V_{q(\mathrm{ref})} = 0.151$ p.u. A three-phase ac circuit breaker connects the inverter to the utility grid at $t = 0.08$ s. Fig. 8 shows the real and reactive power delivered from the PEMFC DG system to the grid when the DG system reaches its steady-state operation from the initial startup. Note that the output steady-state values of P and Q agree with their reference values very well. The corresponding dq components of the inverter output voltage are given in Fig. 9. It is noted that the dq components of the output voltage also reach their prescribed reference values.

The output voltage and current curves of each fuel cell array for this case are shown in Fig. 10. Note that when the system reaches steady state, the fuel cell output current ripple is about 10% and the fuel cell output voltage ripple is less than 3.3%. These relatively small variations of the current and voltage are indicative of the healthy operation of fuel cells [26]. The dc bus voltage (output voltage of the boost dc/dc converter) for this case is shown in Fig. 11. Note that the dc bus voltage comes up to its reference value (480 V) though the fuel cell terminal voltage is much lower than its no-load value under this heavy loading condition (see Fig. 10). The voltage ripple at the dc bus is about 1.25%, which is within the acceptable range.

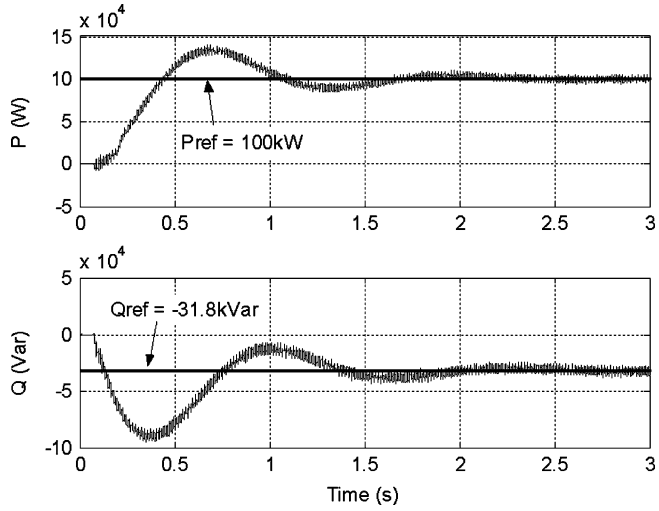

Fig. 12. P and Q delivered to the grid: Light loading.

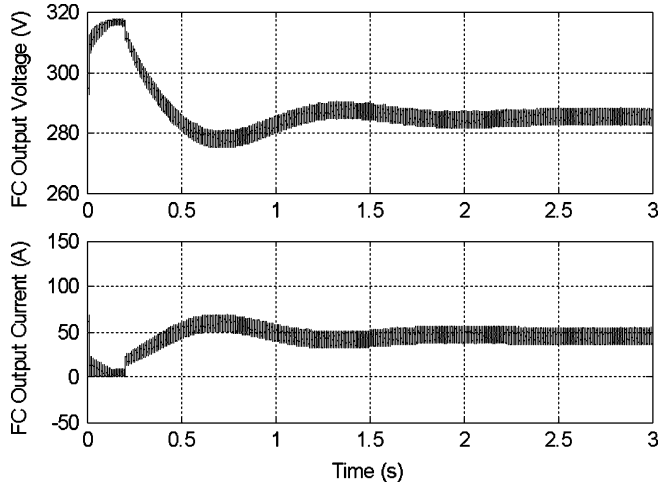

Fig. 13. Output voltage and current of each fuel cell array under light loading.

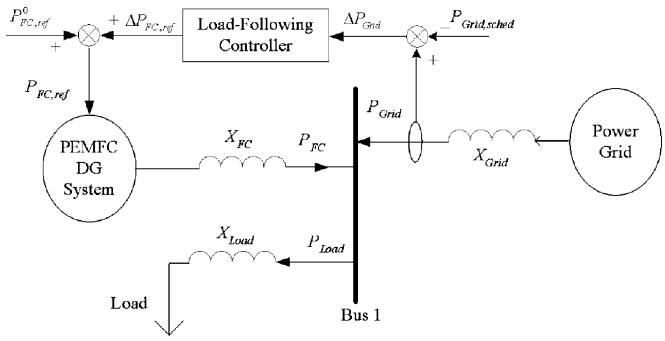

Fig. 14. System for the PEMFC load-following study.

B. Desired P Delivered to the Grid, Q Consumed from the Grid: Light Loading

Under light utility loading, the power required from the fuel cell DG system is normally low, and the DG system may be set to consume the excessive reactive power from the grid, i.e., $Q < 0$. This scenario is examined in this subsection. The reference values of P and Q were set at $P_{\rm ref} = 100$ kW and $Q_{\rm ref} = -31.8$ kVar with an initial step-change startup. The voltage of the utility grid is set to $E = 1.0\angle 0^\circ$ p.u. for this case study. Using equations (7) and (8), the desired amplitude and angle of the filtered output voltage of the inverter turn out to be $V_s = 1.0$p.u., $\delta = 2.648^\circ$. Converting the values into dq coordinates, we get $V_{d(\rm ref)} = 0.99893$ p.u. and $V_{q(\rm ref)} = 0.0463$ p.u.

Fig. 12 shows the real and reactive power responses of the fuel cell DG system. Note that at steady state, the fuel cell power system delivers 100 kW of real power to the grid and consumes 31.8 kVar of reactive power from the grid ($Q = -31.8$ kVar), which match the reference values set for P and Q.

Fig. 13 shows the dc output voltage and current of each fuel cell array under light loading. In this case the fuel cell output current percentage ripple is bigger than that of case A due to lighter loading. However, the fuel cell output voltage ripple is only about 2%, which is even less than that of case A due to a higher steady-state fuel cell output voltage under light loading.

C. Load-Following Analysis

In a fuel cell DG system, a certain amount of power may be scheduled to be delivered to a load center from the utility grid with the rest to be supplied by the fuel cell system. Therefore, a proper load-following controller must be designed to ensure that only scheduled power is delivered from the grid and that the fuel cell system follows the remainder of load demand. In the deregulated power market, the ancillary service costs due to load-following operations can be as high as 20% of the total ancillary service costs [27]. Fig. 14 shows the system for which the load-following study for the PEMFC DG system was carried out. Bus 1 in the figure can be considered as a micro-grid, to which the PEMFC DG system and the power grid are connected to supply power to the load. The power delivered from the grid ($P_{\rm Grid}$) is kept constant ($P_{\rm Grid,sched}$), and the PEMFC DG system is required to follow load as it changes.

The load-following control diagram is also shown in Fig. 14. $P_{\rm Grid}$ is measured and compared with the grid scheduled power. The error ($\Delta P_{\rm Grid}$) is then fed through the load-following controller to generate the adjustment power reference value ($\Delta P_{\rm FC,ref}$), which is added to the initial power reference value ($P^0_{\rm FC,ref}$) to give the new power reference value ($P_{\rm FC,ref}$) for the PEMFC system. Therefore, as load varies, $P_{\rm FC,ref}$ is adjusted to ensure that the fuel cell DG system will compensate the changes of $P_{\rm Load}$. It should be noted that fuel cell power adjustment is assumed to be within the safe operating range of the fuel cell DG system.

In this case study $P_{\rm Grid}$ is set to 100 kW (1 p.u.). As shown in Fig. 15, at the beginning the load is 2 p.u., and therefore the fuel cell system delivers the remaining 1 p.u. power to the load. At $t = 0.3$ s, the load demand steps up to 3 p.u. and drops back to its original value (2 p.u.) at $t = 4.1$ s. It is noted from Fig. 15 that the power grid responds to the initial load changes, and then the PEMFC DG system picks up the load changes to keep the grid power at its scheduled value. The simulation results show that the PEMFC DG system can follow the load power changes in less than 2 s.

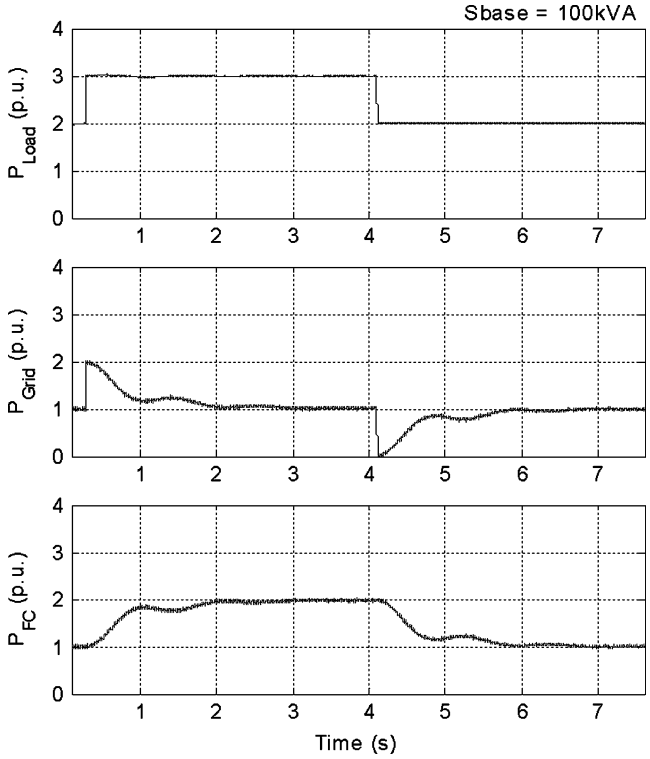

Fig. 15. Power curves of the load-following study.

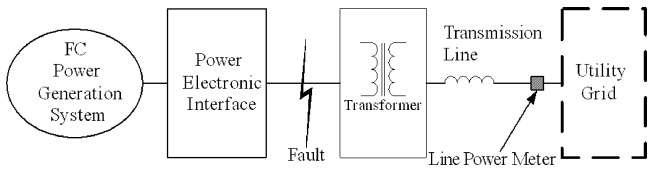

Fig. 16. Faulted fuel cell DG system.

D. Fault Analysis

It is important to know whether the fuel cell DG system will remain stable under fault. The fuel cell system delivers 2 p.u. to the utility grid before the fault. A severe three-phase fault is simulated to occur at $t = 0.7$ s at the low voltage side of the step-up transformer connecting the fuel cell power system to the grid, as shown in Fig. 16. The fault lasts for five cycles (0.0833 s) and is cleared at $t = 0.7833$ s.

The power flow through the transmission line is shown in Fig. 17. During the fault the transmission line power changes direction since the utility grid also supplies power to the faulted point. As shown in the figure, the fuel cell system remains stable after the disturbance. Though the system is stable, there is a rush of power delivered from the fuel cell power plant to the utility grid when the fault is cleared. This is due to the large phase difference between the utility grid and the inverter output voltage when the fault is cleared. One of our future tasks is to add a soft-starting control to limit the peak power when the system recovers from a fault.

One advantage of the two-loop (voltage and current) inverter control is its capability to limit fault currents. To show this advantage, the simulation with the same fault on the system

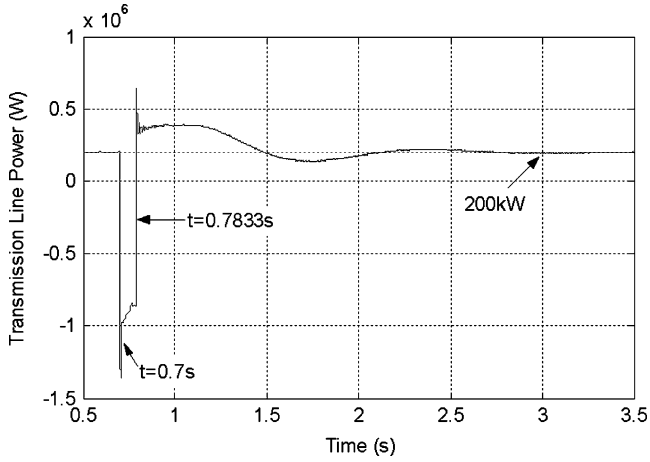

Fig. 17. Faulted PEMFC DG system: Power flow of the transmission line.

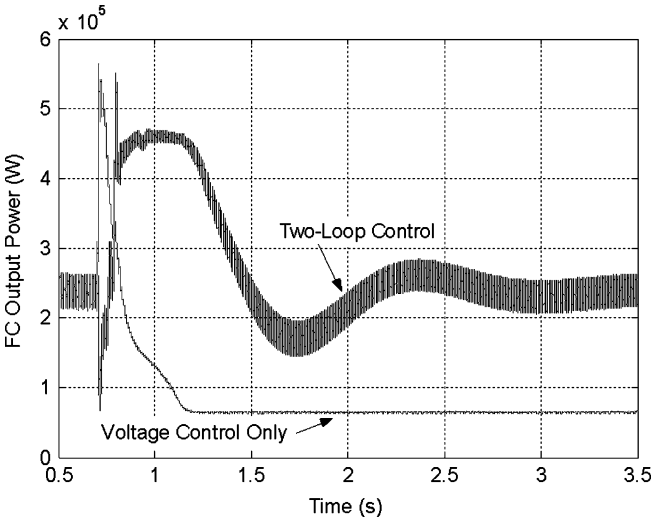

Fig. 18. Faulted PEMFC DG system: Fuel cell output powers for the fault studies.

with only voltage control on the inverter was also conducted for comparison. The fuel cell output power under these two different inverter control strategies is shown in Fig. 18. It is noted that the system cannot remain stable when only the voltage control is applied for inverter control. Because there is no current limit control for this case, the fuel cell output current steps up sharply due to the fault and exceeds the current corresponding to the fuel cell maximum power point. As a result, the fuel cell output power drops sharply. It can be observed from Fig. 18 that the system with two-loop inverter control comes back to the prefault state while the system with only voltage control on the inverter cannot recover to its original state.

VI. Conclusion

Modeling, control, and simulation study of a PEMFC DG system is investigated in this paper. A validated 500-W PEMFC dynamic model, reported in [1], is used to model the fuel cell power plant. The state space models for the boost dc/dc converter and the three-phase inverter are also discussed. Controller

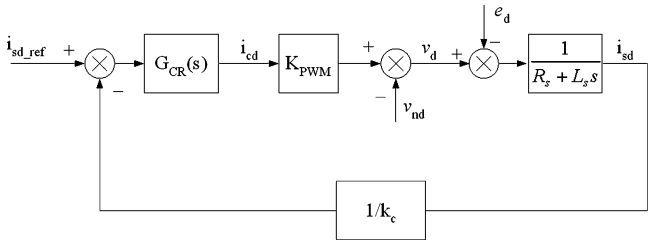

Fig. 19. Block diagram of the current control loop for the inverter.

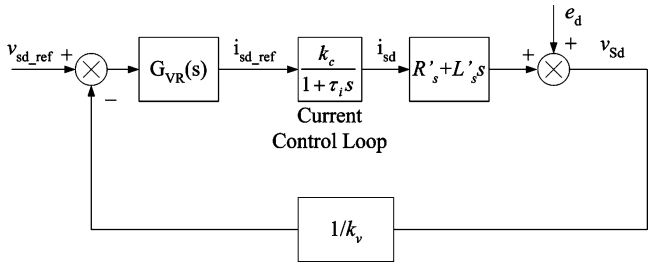

Fig. 20. Block diagram of the voltage control loop for the inverter.

designs for the dc/dc converter and the three-phase inverter are given using linearized small-signal converter/inverter models. Conventional PI voltage feedback controllers are used for the dc/dc converters to regulate the dc bus voltage, and a dq transformed two-loop current control scheme is used on the inverter to control the real and reactive power delivered from the fuel cell system to the utility grid.

A MATLAB/Simulink model of the proposed PEMFC DG system was implemented using the SimPowerSystems blockset. The validity of the proposed control schemes over a large operating range was verified through simulations on nonlinear converter/inverter models. Simulation results of the case studies show that the real and reactive power delivered from the fuel cell system to the utility grid can be controlled as desired while the dc bus voltage is maintained well within the prescribed range. The results also show that the fuel cell system is capable of load-following and can remain stable under the occurrence of severe faults. It is noted that a two-loop inverter control scheme has an advantage over a voltage-only control scheme for the inverter on fault protection and system stability.

APPENDIX

The block diagrams of the simplified current and voltage control loops for the inverter are given in Figs. 19 and 20, respectively. Only d-axis component values are shown in the figures. Controllers for q-axis component values can be designed similarly.

In Fig. 19, $G_{\rm CR}(s) = k_{\rm cp} + k_{\rm ci}/s$ is the current regulator, $K_{\rm PWM}$ is the overall gain of the PWM pulse generator for the inverter; $\frac{1}{R_s + L_s s}$ is the equivalent admittance of the combination of LC filter, power transformer, coupling inductor, and transmission line; and $1/k_c$ is the current transducer ratio.

In Fig. 20, $G_{\rm VR}(s) = k_{\rm vp} + k_{\rm vi}/s$ is the voltage regulator; $\frac{k_c}{1+\tau_i s}$ is the lag approximation for the inner current loop; $R'_s + L'_s s$ is the equivalent impedance of the combination of the power transformer, coupling inductor, and transmission line; and $1/k_v$ is the voltage transducer ratio.

The parameters of the current and voltage controllers are given in Table III.

TABLE III
PARAMETERS OF THE CONTROLLERS FOR THE THREE-PHASE VSI

K_{ci}	K_{cp}	K_{vi}	K_{vp}
250	2.5	25	0.25

ACKNOWLEDGMENT

The author would like to thank to Dr. D. A. Pierre at Montana State University and Dr. H. Mao at Florida Power Electronics Center are acknowledged.

REFERENCES

[1] C. Wang, M. H. Nehrir, and S. R. Shaw, "Dynamic models and model validation for PEM fuel cells using electrical circuits," *IEEE Trans. Energy Conversion*, vol. 20, no. 2, pp. 442–451, Jun. 2005.
[2] C. J. Hatziadoniu, A. A. Lobo, F. Pourboghrat, and M. Daneshdoost, "A simplified dynamic model of grid-connected fuel-cell generators," *IEEE Trans. Power Delivery*, vol. 17, no. 2, pp. 467–473, Apr. 2002.
[3] M. D. Lukas, K. Y. Lee, and H. Ghezel-Ayagh, "Development of a stack simulation model for control study on direct reforming molten carbonate fuel cell power plant," *IEEE Trans. Energy Conversion*, vol. 14, no. 4, pp. 1651–1657, Dec. 1999.
[4] J. Padullés, G. W. Ault, and J. R. McDonald, "An integrated SOFC plant dynamic model for power system simulation," *J. Power Sources*, pp. 495–500, 2000.
[5] K. Sedghisigarchi and A. Feliachi, "Dynamic and transient analysis of power distribution systems with fuel cells—Part I: Fuel-cell dynamic model," *IEEE Trans. Energy Conversion*, vol. 19, no. 2, pp. 423–428, Jun. 2004.
[6] K. Sedghisigarchi and A. Feliachi, "Dynamic and transient analysis of power distribution systems with fuel cells—Part II: Control and stability enhancement," *IEEE Trans. Energy Conversion*, vol. 19, no. 2, pp. 429–434, Jun. 2004.
[7] Z. Miao, M. A. Choudhry, R. L. Klein, and L. Fan, "Study of a fuel cell power plant in power distribution system—Part I: Dynamic model," in *Proc. IEEE PES General Meeting*, Denver, CO, Jun. 2004.
[8] Z. Miao, M. A. Choudhry, R. L. Klein, and L. Fan, "Study of a fuel cell power plant in power distribution system—Part II: Stability control," in *Proc. IEEE PES General Meeting*, Denver, CO, Jun. 2004.
[9] D. Candusso, L. Valero, and A. Walter, "Modelling, control and simulation of a fuel cell based power supply system with energy management," *Proc. IECON*, vol. 2, pp. 1294–1299, 2002.
[10] R. Naik, N. Mohan, M. Rogers, and A. Bulawka, "A novel grid interface, optimized for utility-scale applications of photovoltaic, wind-electric, and fuel-cell systems," *IEEE Trans. Power Delivery*, vol. 10, no. 4, pp. 1920–1926, Oct. 1995.
[11] W. Shireen and M. S. Arefeen, "An utility interactive power electronics interface for alternate/renewable energy systems," *IEEE Trans. Energy Conversion*, vol. 11, no. 3, pp. 643–649, Sep. 1996.
[12] G. Spiazzi, S. Buso, G. M. Martins, and J. A. Pomilio, "Single phase line frequency commutated voltage source inverter suitable for fuel cell interfacing," in *Proc. 33rd Ann. IEEE Power Electron. Specialists Conf.*, vol. 2, 2002, pp. 734–739.
[13] K. Ro and S. Rahman, "Control of grid-connected fuel cell plants for enhancement of power system stability," *Renewable Energy*, vol. 28, no. 3, pp. 397–407, Mar. 2003.
[14] H. Komurcugil and O. Kukrer, "A novel current-control method for three-phase PWM ac/dc voltage-source converters," *IEEE Trans. Ind. Electron.*, vol. 46, no. 3, pp. 544–553, Jun. 1999.
[15] N. Mohan, T. M. Undeland, and W. P. Robbins, *Power Electronics: Converters, Applications, and Design*. New York: Wiley, 2003.
[16] D. W. Hart, *Introduction to Power Electronics*. Englewood Cliffs, NJ: Prentice Hall, 1997.

[17] M. H. Todorovic, L. Palma, and P. Enjeti, "Design of a wide input range DC-DC converter with a robust power control scheme suitable for fuel cell power conversion," in *Proc. 19th Ann. IEEE Appl. Power Electron. Conf.*, Anaheim, CA, 2004.
[18] S. M. N. Hasan, S. Kim, and I. Husain, "Power electronic interface and motor control for a fuel cell electric vehicle," in *Proc. 19th Ann. IEEE Appl. Power Electron. Conf.*, Anaheim, CA, 2004.
[19] *Fuel Cell Handbook*, EG&G Services, Parsons Inc., Washington, DC, Oct., 2000. DOE of Fossil Energy, National Energy Technology Lab.
[20] J. Larminie and A. Dicks, *Fuel Cell Systems Explained*. New York: Wiley, 2001.
[21] J. Van de Vegte, *Feedback Control Systems*, 3rd ed., Englewood Cliffs, NJ: Prentice Hall, 1994.
[22] *IEEE Standard for Interconnecting Distributed Resources with Electric Power Systems*, IEEE Standard 1547, 2003.
[23] M. Tsai and W. I. Tsai, "Analysis and design of three-phase AC-to-DC converters with high power factor and near-optimum feedforward," *IEEE Trans. Ind. Electron.*, vol. 46, no. 3, pp. 535–543, Jun. 1999.
[24] H. Mao, "Study on three-phase high-input-power-factor PWM-voltage-type reversible rectifiers and their control strategies," Ph.D. dissertation, Zhejiang Univ., Hangzhou, Zhejiang, China, 2000. (in chinese).
[25] J. D. Glover and M. S. Sarma, *Power System Analysis and Design*, 3rd ed., Pacific Grove, CA: Brooks/Cole, 2002.
[26] R. S. Gemmen, "Analysis for the effect of inverter ripple current on fuel cell operating condition," *Trans. ASME—J. Fluids Eng.*, vol. 125, no. 3, pp. 576–585, May 2003.
[27] Y. Zhu and K. Tomsovic, "Development of models for analyzing the load-following performance of microturbines and fuel cells," *J. Elect. Power Syst. Res.*, vol. 62, no. 1, pp. 1–11, May 2002.
[28] R. Wu, T. Kohama, Y. Kodera, T. Ninomiya, and F. Ihara, "Load-current-sharing control for parallel operation of DC-to-DC converters," in *Proc. IEEE PESC'*, Seattle, WA, Jun. 1993, pp. 101–107.
[29] P. C. Krause, O. Wasynczuk, and S. D. Sudhoff *Analysis of Electric Machinery*, Piscataway, NJ: IEEE Press, 1995.
[30] J. G. Kassakian, M. F. Schlecht, and G. C. Verghese, *Principles of Power Electronics*. Reading, MA: Addison-Wesley, 1991.

C. Wang (S'02) received the B.S. and M.S. degrees in electrical engineering from Chongqing University, Chongqing, China, in 1994 and 1997, respectively. He is currently pursuing the Ph.D. degree at Montana State University, Bozeman.

From 1997 to 2002, he was as an Electrical Engineer with Zhejiang Electric Power Test and Research Institute, Hangzhou, China. His current research interests include modeling and control of power systems and electrical machinery, alternative energy power generation systems, distributed generation, and fault diagnosis and online monitoring of electric machinery.

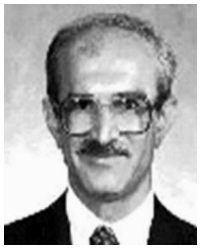

M. H. Nehrir (M'88–SM'89) received the B.S., M.S., and Ph.D. degrees in electrical engineering from Oregon State University, Corvalis, OR, in 1969, 1971, and 1978, respectively.

Since 1987, he has been a full Professor in the Electrical and Computer Engineering Department at Montana State University, Bozeman. His primary areas of interest are modeling and control of power systems and electrical machinery, alternative energy power generation systems, distributed generation, and application of intelligent controls to power systems. He is the author of two textbooks and an author or coauthor of numerous technical papers.

H. Gao (S'98–M'02) received the B.S. and M.S. degrees from Tsinghua University, Beijing, China, in 1990 and 1993, respectively, and the Ph.D. degree from Texas A&M University, College Station, in 2001, all in electrical engineering.

Since August 2002, he has been a Faculty Member in the Electrical Engineering Department at Montana State University, Bozeman. His research interests include electric machines, motor drives, power electronics, electric and hybrid electric vehicles, and renewable source power systems.

Dr. Gao is a member of the Power Electronics Society, Industry Applications Society, and Industrial Electronics Society.